Journal of Heat and Mass Transfer Research

Journal homepage: https://jhmtr.semnan.ac.ir

Semnan University

ISSN: 2383-3068

Research Article

Prediction and Optimization of Viscosity of Ethylene Glycol based ZnO Nanofluids using Response Surface Methodology (RSM)

Behrouz Raei

Department of Chemical Engineering, Mahshahr Branch, Islamic Azad University, Mahshahr, Iran

ARTICLE INFO

Article history:

Received: 2025-03-14

Revised: 2025-05-13

Accepted: 2025-05-23

Keywords:

Response surface methodology;

Viscosity;

Nanofluid;

Modeling;

Stability.

ABSTRACT

Since nanofluid science is still fairly new, the properties of numerous nanofluids have not been fully studied. Consequently, equations for precise calculations in this field are not yet available. The present research predicts the viscosity ratio (VISR) of stabilized ethylene glycol-based ZnO nanofluids using the response surface methodology (RSM). This research was conducted under experimental conditions, utilizing solid volume fractions (SVF) ranging from SVF=0.01% to SVF=0.15%, and temperatures between T=20°C and T=60°C. Various models were assessed according to a set of quality indicators and plots. Upon reviewing the quality indicators and plots for various models, the cubic model was determined to be the most suitable option. The values of standard deviation (std.dev), coefficient of determination (R^2) and coefficient of variation (C.V) for the cubic model were 0.0060, 0.9831, and 0.5426, respectively. Also, the adjusted R^2 and predicted R^2 parameters of the cubic model were equal to 0.9679 and 0.9492 respectively, which signifies the accuracy of the model. The results of the RSM model were compared with more than 25 equations available in the literature. The outcomes showed that the RSM model had the lowest error as average absolute relative deviation (AARD=2.9%) in predicting the VISR of nanofluid. Ultimately, the best state of VISR of nanofluid in the conditions of SVF= 0.01%, and T = 20°C value was 1.070. The application of RSM cuts down on experimental costs and time, in addition to helping identify the most suitable model.

1. Introduction

Currently, heating systems that are both cost-effective and eco-friendly are considered vital in many industries [1-4]. Moreover, due to different increment techniques aimed at improving the performance of engineering networks, numerous investigators are investigating the application of nanoparticles to boost the performance of networks [5-7]. In light of the pressing demand to save energy and preserve the environment, as well as its important role in the global context, addressing challenges including improving heat transfer efficiency to obtain the best performance, decreasing fuel usage, and minimizing air pollution is of considerable significance [8-10]. One suitable method to enhance the heat transfer rate is by employing fluids that possess superior heat capacities in comparison to traditional fluids like water, ethylene glycol (EG), and oil [11] and can function as an intelligent fluid in heat transfer challenges

*** Corresponding author.**
E-mail address: behrouz.raei@iau.ac.ir

Cite this article as:

Raei, B., 2026. Prediction and Optimization of Viscosity of Ethylene Glycol based ZnO Nanofluids using Response Surface Methodology (RSM). *Journal of Heat and Mass Transfer Research*, 13(1), pp. 101-118.

https://doi.org/10.22075/JHMTR.2025.37095.1689

to demonstrate significant heat transfer capability [12-15]. Intelligent fluids are constructed of nanoparticle suspensions, with particle dimensions typically below 100 nanometers, dispersed within base fluids such as water, oil, or EG [16]. In earlier times, traditional fluids were employed for the purpose of heat transfer. As science and technology evolved over time, researchers utilized solid microparticles to enhance the thermal conductivity in traditional fluids and achieved a growth in heat transfer rates. Nonetheless, applying these millimeter and microtiter particles results in issues like wear on the flow channel or a decrease in fluid pressure. Consequently, the investigators employed nanoparticles to address the issues arising from the microparticle application and additionally enhance the transfer rate in traditional fluids. To achieve high performance in thermal systems, investigators examined various types of nanofluids to acquire a deeper insight into the thermophysical characteristics of these fluids [17, 18]. Among the thermophysical characteristics of nanofluids, viscosity reflects the resistance of the fluid. As a result, viscosity has been identified as a critical factor affecting the performance and efficiency of energy systems [19, 20]. In the context of industrial machinery and scientific research involving heat transfer processes, the viscosity of nanofluids plays a key role in determining the flow characteristics, pumping power requirements, pressure drop, and overall operational efficiency of systems [21-23]. Therefore, the accurate determination and estimation of nanofluids viscosity is very significant. Various researches have been conducted in this field, which can be referred to review papers [24, 25]. Numerous types of metallic oxide nanoparticles have been utilized as additives in nanofluids to date. Among the various additives, CuO, Al_2O_3, TiO_2, and Fe_3O_4 are the most extensively studied. The viscosity of nanofluids containing these particles is more likely to exhibit a consistent and widely agreed-upon behavior. Nevertheless, the examination of EG-based ZnO nanofluids has not been well explored.

A detailed examination of the viscosity of nanofluids containing ZnO nanoparticles in different base fluids is presented in Table 1.

Table 1. Review on viscosity of nanofluids with ZnO nanoparticles

Researcher Detail	Base fluid	Particle size (nm)	Particle concentration	Remarks
Esfe and Saedodin [26]	EG	18	0.25-5% volume fraction	The nanofluid dynamic viscosity increases considerably with particle volume fraction but does not significantly change (decrease) with increasing temperature.
Yalcin et al. [27]	Water	20&50~150	0.5-1% volume fraction	The maximum relative viscosity was measured for 1% ZnO (50~150 nm) at 1.35 times water.
Li et al. [28]	EG	30	1.75-10.5% mass fraction	It shows that ZnO/EG nanofluids with mass fraction wt.% ≦ 10.5 demonstrate Newtonian behavior.
Pastoriza-Gallego et al. [29]	EG	40 to 100 &4.6	0.5-4.7% volume fraction	Viscosity increases with concentration a usual for this type of dispersion and decreases with temperature.
Gamal et al. [30]	EG/W(50:50)	20	0.25-1% volume fraction	The maximum augmentation for 1% ZnO-EG/W (50:50) nanofluid is 45.1%.
Siddiqi et al. [31]	Deionized water	20	0.012-0.048% mass fraction	The viscosity was directly related to the nanoparticle loading while inversely proportional to nanofluids temperature.
Cabaleiro et al. [32]	EG/W(50:50)	40-100	1-5% mass fraction	Dynamic viscosity rises strongly with nanoparticle concentration.
Sharma et al. [33]	Water	30	0.01-0.2% volume fraction	The results evidenced that the absolute viscosity of the water was augmented by 1.43% through the diffusion of 0.2 vol% of nano-ZnO particles in water.
Jeong et al. [34]	Water	90-210&20-40	0.05-5% volume fraction	The viscosity of the nanofluids increased with increases in the volume concentration by up to 69%.

As stated in the previously mentioned publications, there exist a variety of empirical data in the area of nanofluid viscosity that have examined various influential parameters. Even though these models are not grounded in theoretical principles, they are commonly employed in engineering practices owing to their straightforward application and ability to effectively align with experimental results [35]. It is essential to conduct a thorough analysis of these experimental data to derive valid conclusions regarding nanofluids performance and efficiency. In this context, several initiatives have been undertaken to model the empirical data [36-41], focusing on the optimization of various functions and the assessment of the impact of different variables. Numerous algorithms including RSM, artificial neural network (ANN), genetic algorithm (GA), independent component analysis (ICA), particle swarm optimization (PSO), non-dominated sorting genetic algorithm (NSGAII) and artificial intelligence (AI) have been utilized to optimize certain parameters like the performance of nanofluids, thermal conductivity, viscosity, and pressure drop, etc. Using 15 machine learning algorithms, the rheological behavior of oil SAE40-based nano-lubricant in the presence of MWCNT and MgO nanoparticles was predicted by Baghoolizadeh et al. [42]. The machine learning algorithms demonstrated strong predictive capability, with the model outputs showing excellent agreement with experimental results. Prediction of ethylene glycol-based ZnO nanofluidic heat transfer versus magnetic effect by deep learning was conducted by Demirpolat & Baykara [43]. The findings indicated that deep learning models could predict heat transfer coefficients well. Also, references [44-48] have used machine learning to predict the thermophysical properties of nanofluids. In the study by Demirpolat & Uyar [49] , the heat transfer coefficient (h) was determined utilizing MgO nanoparticles dispersed in base fluids of pure water, ethanol, and ethylene glycol within a nanofluid experimental setup. In the continuation of the experimental study, the variation of the heat transfer coefficient according to the Reynolds number was examined through experimental modeling in the ANSYS program using MgO nanofluid. The computational results demonstrated that the incorporation of MgO nanofluid into the system yields a significant enhancement in heat transfer performance when compared to pure water. Mahanta and Sharma [50] conducted a numerical investigation of unsteady rotating flow characteristics in Casson tetra hybrid nanofluids, incorporating dual stratification effects while analyzing the influence of variable thermal conductivity and thermal stratification on heat transfer performance. The thermophysical properties of the tetra nanoparticles, i.e., Ag, Cu, SWCNTs, and MWCNTs, comprise of a C2H6O2–H2O (50–50%) base fluid. The numerical results demonstrate that rotation and stretching significantly affect velocity and temperature profiles. The study employs RSM with multiple linear regression to statistically evaluate the influence of key parameters on both the drag coefficient and energy transfer rate across the linearly elongated surface. These relationships are further visualized through three-dimensional surface plots to elucidate parametric interactions. We can also refer to other research [51-65] which has used numerical methods and RSM to investigate the properties and efficiency of nanofluids. Chu et al. [66] conducted experimental studies and employed RSM and ANN modeling to analyze the rheological properties of a MWCNT-TiO_2/5W40 hybrid nanofluid. The findings indicated that the nanofluid's viscosity increased as the shear rate and temperature reduced, along with a rise in volume fraction. The existence of nanoparticles increased the viscosity of the nanofluid by as much as 790%. Prediction of viscosity values of nanofluids at different pH values by alternating decision tree and multilayer perceptron methods was studied by Demirpolat & Das [67]. Nanofluids were prepared by dispersing CuO nanoparticles in pure water, ethanol, and ethylene glycol, and their viscosity was experimentally measured. Various computational intelligence techniques were employed to develop predictive models for nanofluid viscosity values. The accuracy of the predictive model was assessed using error metrics, including mean square error (MSE), root mean square error (RMSE), and mean absolute percentage error (MAPE). The Multilayer Perceptron method demonstrated the lowest error values among the computational approaches and was consequently selected as the optimal predictive model. Esfe et al. [68] examined the dynamic viscosity of a HNF composed of MWCNT (40%) and SiO_2 (60%) dispersed in 5W50 oil, utilizing both experimental and statistical approaches. By employing two methodologies—ANN and statistical correlation—, they established a relationship between the dynamic viscosity of the HNF and the independent variables. Several studies in the literature have employed ANN to predict nanofluids thermophysical properties, as demonstrated in references [69-78].

RSM is regarded as the most favored statistical method for optimizing the key variables of any real-time manufacturing process, as it necessitates a minimal number of

experiments and delivers optimal condition settings to achieve maximum yield [79, 80]. Esfe et al. [41] conducted a comparable analysis of different RSM models to predict the dynamic viscosity of a HNF consisting of 60% SiO_2 and 40% MWCNT dispersed in SAE40 oil as the base fluid. After evaluating the quality metrics and graphical representations of multiple models, the quartic model was identified as the most appropriate choice. In a separate study conducted by Esfe et al. [81], RSM was employed to optimize the thermal characteristics and rheological characteristics of an Al_2O_3-EG/water (20:80) nanofluid. Based on the findings, over 99% of the variations in viscosity and thermal conductivity of the nanofluid were able to be forecasted by the models, indicating that the utilized model is accurate. Esfe et al. [82] examined the dynamic viscosity of a 10W40 oil-based HNF including MWCNT (40%) and TiO_2 (60%). RSM was effectively implemented in this study and offered correlations to precisely forecast the nanofluid's viscosity. The evaluation of statistical metrics and visual representations indicated that the fifth-order model exhibited superior performance compared to the alternative models. Esfe et al. [83] examined the dynamic viscosity of a hybrid nanofluid composed of MWCNT-Al_2O_3 in a 40:60 ratio dispersed in SAE50 oil. Nanofluids viscosity modeling is also conducted utilizing the RSM. Multiple models are presented, and the optimal model is chosen based on the criteria for R^2, adjusted R^2, predicted R^2, and std.dev. The findings indicate that the fifth-order model achieved values of 0.9997, 0.9997, 0.9996, and 2.39 for the R^2, adjusted R^2, predicted R^2, and std.dev parameters, respectively, indicating a highly accurate representation of the modeling process. Esfe et al. [39] explored the rheological properties of a HNF consisting of MWCNT-SiO_2 in a 10:90 ratio using the RSM. The study's primary objective was to develop a novel correlation between these properties. Khetib et al. [84] employed RSM to explore the viscosity of a paraffin-based CuO nanofluid. Experiments carried out at T=25–100°C and mass fractions of 0.25-6% provided the data used in the modeling. RSM indicates that in comparison to linear polynomials and second degree polynomials, the findings derived from third degree polynomials are more precise. Also, references [85-87] have used RSM to predict the thermophysical properties of nanofluids.

In the current investigation, the dynamic viscosity of ZnO/EG nanofluid was experimentally investigated across a range of SVF and T. In the experimental part, the stability characteristics of nanofluid and the influence of SVF and T on the viscosity of nanofluid are examined. The literature review shows that linear and nonlinear regression techniques have been widely used by various researchers. But there is no study in which the ability of RSM method to estimate ZnO/EG nanofluid viscosity is compared. So, in the statistical section, utilizing Design Expert software (version 13.0.0), RSM will be employed to establish a correlation and develop an experimental model aimed at predicting experimental outcomes. Therefore, in this study, the accuracy of the RSM method of estimating the viscosity ratio (VISR) is challenged. This approach will facilitate the examination of the relationship between the independent variables, namely T and SVF, and the dependent variable, viscosity. Different models, such as 2FI, quadratic, cubic, and quartic modeling, were suggested to estimate the viscosity of nanofluids utilizing R^2, adjusted R^2, predicted R^2, adeq precision and std.dev, which determined the accuracy of the model; the best model was selected. After the model was chosen, it underwent review and analysis, and several plots including the comparison of predicted and actual values, normal distribution, residual values, and the Box-Cox plot were presented. The optimal nanofluid viscosity was established based on the chosen model. The final goal of this research was to compare the outcomes of the estimation of the RSM model with other models (25 models) presented in the literature. In addition to the accuracy and speed of access to the results, the RSM model offers an industry advantage. This conserves time and money and greatly assists industries that utilize ZnO/EG nanofluid.

2. Experimental Methodologies

2.1. Nanofluid Preparation

One-step and two-step approaches are frequently utilized methods for the synthesis of nanofluids. The present research employs the two-step method. The specifications for zinc oxide nanoparticles, sourced from US Research Nanomaterials, Inc., are presented in Table 2. The depiction is in Fig. 1 (Transmission Electron Microscopy (TEM)) clearly indicates that the nanoparticles exhibit a nearly spherical morphology.

Table 2. Specification of nanoparticle used in this study

Nanoparticle	Zinc Oxide
Average particle size (nm)	10-30
Purity	>99%
Density (kg/m3) True	5606
Color	Milky white
Morphology	Nearly spherical
Specific area (m2/g)	20-60
Specific heat (J /kg K)	514
Thermal conductivity(W/m K)	29

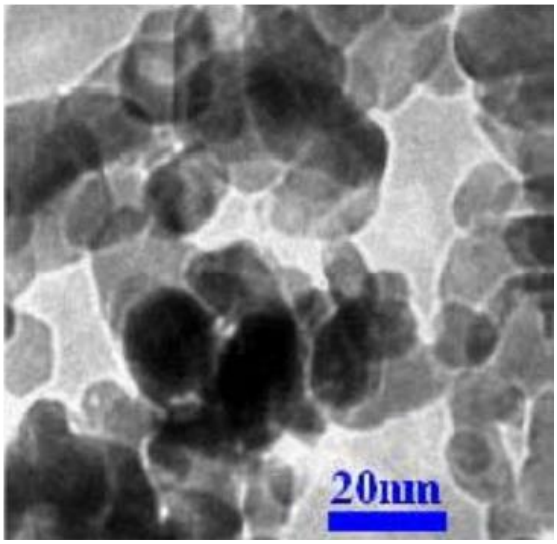

Fig. 1. Powder TEM pattern for ZnO nanoparticles

In this research, the selected concentrations of the nanofluids were 0.01, 0.05, 0.1, and 0.15 vol%, along with temperatures of 20, 30, 40, 50, and 60 °C. The initial step involved measuring the characteristic mass of the nanoparticles (0.05606, 0.2803, 0.5606, and 0.8409 mg) using a highly accurate digital microbalance, which provides readings to four decimal places. Subsequently, 100 ml of EG was added to the ZnO nanoparticles. Thereafter, to achieve uniform dispersion, the nanofluids underwent magnetic stirring for 1 h at 1000 rpm. To enhance the dispersion stability of the synthesized nanofluids, an ultrasonic water bath (produced by BANDELIN, operating at a power of 240 W and a frequency of 35 kHz) was utilized for 1 h. Ultimately, the nanofluids underwent 30 min of magnetic stirring to promote improved dispersion stability. Nanofluids stability is an increasing concern, and researchers have employed various methods for its proper examination [88]. In this study, dispersion stability was assessed using a visual photography method, which involved analyzing the transparent regions of the nanofluids observed in the upper section of the glass vial over the course of the investigation. Initially, the glass vial was partitioned into equal segments by positioning an accurate scale over it, and subsequently, the transparent part of the fluid was assessed meticulously to establish the rate at which the nanoparticles were settling. The technique is straightforward and commonly employed to assess nanofluids stability, as indicated in the literature [12, 13, 89, 90]. Different images were taken at consistent times using a high-resolution and magnifying digital camera. Then the captured images were analyzed to evaluate the stability of nanofluids [91]. Figure 2 illustrates the outcomes of the visual examination performed on the samples following a duration of 48 h. The examination revealed no evidence of sedimentation after 48 h without the addition of any surfactants. The likely explanation is the existence of significant electrostatic repulsion forces among nanoparticles due to their reduced size. The results of the current study conform with research carried out on ZnO/EG nanofluids [26, 28, 29].

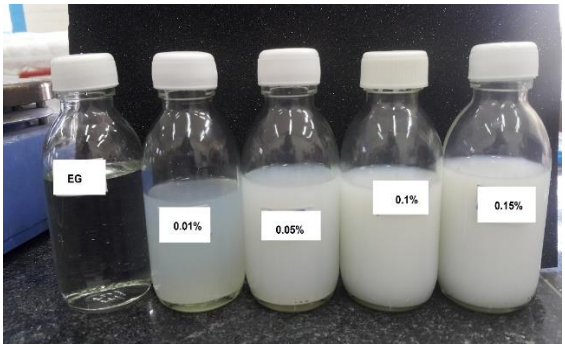

Fig. 2. Stability analysis by visual inspection for ZnO/EG nanofluid after 48 h

2.2. Measurement of Viscosity

Figure 3 illustrates an experimental apparatus designed to measure ZnO/EG nanofluids viscosity. In this type of viscometer, viscosity is determined by measuring the time required for a fixed volume of the test liquid to flow through a capillary tube under the influence of gravitational forces at a maintained constant temperature. The apparatus comprises an Ostwald viscometer situated in a temperature-controlled water bath (MATEST model B052-01, Italy) with a temperature fluctuation of ±0. 5 °C. The viscometer is filled with the necessary volume of test fluid (nanofluid) and permitted to flow between two designated marks, A and B (Illustrated in Fig. 3), via the capillary tube. A stopwatch featuring an accuracy of 0.01 s was utilized to measure the time taken to reach the markers on the viscometer.

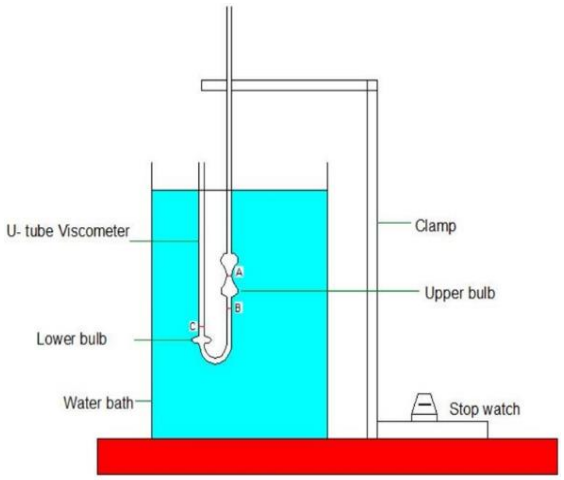

Fig. 3. Schematic of the apparatus for viscosity measurement

Once the viscosity of the base fluid (bf) was known, the viscosity of nanofluids (nf) was calculated using Eqs. (1) and (2):

$$\frac{\mu_{nf}}{\mu_{bf}} = \frac{\rho_{nf}}{\rho_{bf}} \frac{t_{nf}}{t_{bf}} \quad (1)$$

$$\rho_{nf} = \Phi\rho_{np} + (1-\Phi)\rho_{bf} \quad (2)$$

The calibration of the viscometer was verified by measuring the viscosity of distilled water (DW) at the designated test temperatures: 20, 30, 40, 50, and 60 °C. The measured viscosity values for DW were compared with reference data provided by IAPWS[1] in 2008. The maximum percentage error was calculated to be 4.1%. In order to eliminate experimental error and check repeatability, each measurement was repeated 4 times under identical conditions. The final results are presented as the mean of the measurements. The uncertainty in viscosity measurements was estimated based on the accuracy of the instruments. The uncertainty in measuring the viscosity of nanofluids was calculated using the following mathematical relations (Eq. (3)) [92]:

$$U_{\mu nf} = \pm\sqrt{\left(\frac{\Delta\mu_{nf}}{\mu_{nf}}\right)^2 + \left(\frac{\Delta w}{w}\right)^2 + \left(\frac{\Delta T}{T}\right)^2 + \left(\frac{\Delta t}{t}\right)^2} \quad (3)$$

where U represents the uncertainty in measurements; w denotes nanoparticle weight, and T denotes temperature. Δ presents the deviation from measurement. The maximum uncertainty in the measured viscosity was 2.1%.

3. RSM

By employing a range of mathematical and statistical techniques, RSM can be applied to various processes. This method is utilized in the development, formulation, design, and optimization of new products. In this approach, one or more independent variables are presented, along with one or more dependent variables or responses. The objective of the method is to statistically analyze how dependent variables change in response to variations in independent variables. In product development, the response variable is symbolized as y, and the dependent or input variables are denoted as ξ_1, ξ_2, …, ξ_k. To generate a model and illustrate a mathematical relationship, y must be defined as a function of the input variables. Consequently, it is transformed into Eq. (4):

$$y = f(\xi_1.\ \xi_2.\ \ldots.\ \xi_k) + \varepsilon \quad (4)$$

In Eq. (4), ε represents the term that accounts for variables not included in f, which may introduce an error. The term ε encompasses measurement errors as well as a range of intrinsic problems associated with the system or process. Since the actual form of the response function (f) is unknown, it must be approximated using (η). RSM implementation depends on the experimenter's ability to provide precise raw data, as these form the basis for calculations and statistical modeling. Polynomial functions are typically utilized to model processes. These functions resemble first- or second-order equations. In Eq. (5) a first-order model is provided.

$$\eta = \beta_0 + \beta_1 x_1 + \beta_2 x_2 \quad (5)$$

But a first order equation typically resembles Eq. (6).

$$\eta = \beta_0 + \beta_1 x_1 + \beta_2 x_2 + \beta_{12} x_1 x_2 \quad (6)$$

However, the second order model may be expressed as Eq. (7):

$$\eta = \beta_0 + \sum_{i=1}^{n} \beta_i x_i + \sum_{i=1}^{n} \beta_{ii} x_{ii}^2 + \sum_{i<j=1}^{n} \beta_{ij} x_i x_j \quad (7)$$

Higher-order models are also used in RSM. RSM outputs are considered valid and practical only if they accurately predict response values with minimal error.

4. Results and Discussion

4.1. Statistical Evaluation

As illustrated in Fig. 4, the VISR (viscosity ratio, (μnf/μbf)) rose as the SVF of the ZnO/EG nanofluid increased. Conversely, at a fixed SVF, with an augmented T, the VISR of the fluid does not noticeably change. On the other hand, at a constant SVF, as T rises, the VISR of the fluid remains approximately unchanged. The viscosity rises at increasing SVF as a result of enhanced particle aggregation and the development of chain-like structures. Particle agglomeration had a direct effect on the viscosity of nanofluid [23]. The results indicated are consistent with the findings presented in references [26, 28, 30, 93]. The maximum enhancement noted in the viscosity of the ZnO/EG nanofluid is approximately 17% compared to pure EG at SVF of 0.15%.

[1] International Association for the Properties of Water and Steam

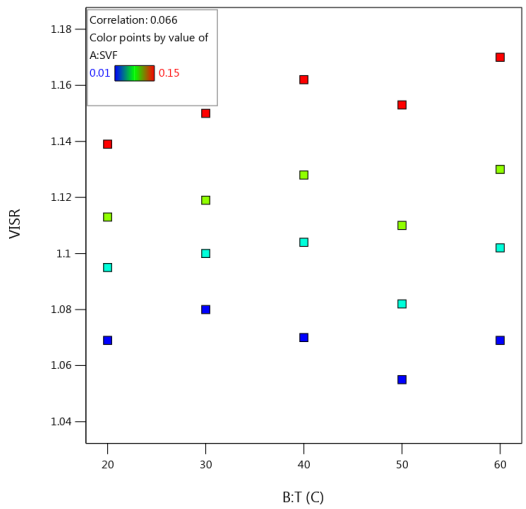

Fig. 4. VISR (a) versus temperature for various solid volume fraction

Data were gathered from 20 experimental tests. In the modeling process, two factors that affect the viscosity ratio (VISR) were recognized: SVF and T. Information pertaining to these factors and their associated coded values is available in Table 3. The study aims to establish a correlation that can predict the VISR of the ZnO/EG nanofluid. Consequently, the response variable in this context is VISR. Different models are examined to determine the most effective option.

Table 4 displays the p-values, adjusted R^2, and predicted R^2 values for the linear model, the two-factor interaction (2FI) model, along with the quadratic and cubic models assessed during analysis.

The column displaying sequential p-values displays the importance level of each term in the model as they were progressively incorporated into the model. A p-value below 0.05 denotes that the term is statistically significant, suggesting that it has an effect on the variability of the response variable [94]. Adjusted R^2, a modified version of R^2, enhances accuracy and reliability by accounting for the influence of extra independent variables that can distort R^2 measurements. A higher adjusted R^2 value demonstrates a better fit between the model and the data. Unlike the adjusted R^2, the predicted R^2 measures how effectively a regression model estimates the responses to new data. While the adjusted R^2 can indicate an accurate model that fits the existing data, the predicted R^2 assesses the likelihood of the model maintaining accuracy for future data. The data presented in this table indicate that the cubic model exhibits the highest adjusted R^2 value of 0.9679 and a predicted R^2 of 0.9492, demonstrating that it is the most accurate model. Table 5 shows the findings from the cubic model analysis of variance (ANOVA). The model's F-value is 64.75, which is significantly higher than 0. 0001. The importance of each element was likewise assessed through the F-value and p-value. A p-value of under 0.05 signifies an important model condition, while parameters with p-values exceeding 0.1 possess little significance. As a result, it is feasible to remove insignificant elements from the model. The greater the F-value and the smaller the p-value, the more significant the associated coefficient term is. In this situation, the A-solid volume fraction and B-temperature model parameters were significant, exhibiting F-values of 23.69 and 9.42, respectively.

Table 6 shows the cubic model fit statistics. The table signifies that the predicted R2 value of 0.9492 is approximately aligned with the adjusted R^2 value of 0.9679, exhibiting a difference of less than 0.0188. This implies that the model can be relied upon for forecasting future observations. Adequate precision (Adeq Precision) evaluates the model's quality by measuring the ratio of data variation to the variation predicted by the model. The adeq precision is a signal-to-noise ratio. It evaluates the relationship between the range of predicted values at design points and the average prediction error. Ratios exceeding 4 signify sufficient model discrimination. The computed ratio of 26.4159 signifies that the model is appropriate for exploring the design space.

Incorporating the experimental data into the RSM processing model aids in creating an equation as shown in Eq. (8).

$$\begin{aligned} VISR = {} & 0.914290 + 0.849271 * SVF \\ & +0.013650 * T + 0.008117 * SVF * T \\ & -8.73538 * SVF^2 - 0.000379 * T^2 \\ & +0.015147 * SVF^2 * T \\ & -0.000052 * SVF * T^2 + 34.69841 * SVF^3 \\ & +3.18750 * 10^{-6} * T^3 \end{aligned} \quad (8)$$

The equation, formulated in terms of actual factors, can predict the response at specific levels of each factor.

Table 3. Specifications of used factors in modeling

Factor	Name	Units	Minimum	Maximum	Coded Low	Coded High	Mean	Std. Dev.
A	SVF	%	0.0100	0.1500	-1 ↔ 0.01	+1 ↔ 0.15	0.0775	0.0540
B	T	C	20.00	60.00	-1 ↔ 20.00	+1 ↔ 60.00	40.00	14.51

Table 4. Summary of statistics for the various models

Source	Sequential p-value	Adjusted R^2	Predicted R^2	
Linear	< 0.0001	0.9205	0.9008	
2FI	0.0198	0.9405	0.9271	
Quadratic	0.9790	0.9322	0.9063	
Cubic	0.0189	0.9679	0.9492	Suggested
Quartic	0.0124	0.9919	0.9715	Aliased

Table 5. ANOVA outcome for the suggested cubic model

Source	Sum of Squares	df	Mean Square	F-value	p-value	
Model	0.0211	9	0.0023	64.75	< 0.0001	significant
A-SVF	0.0009	1	0.0009	23.69	0.0007	
B-T	0.0003	1	0.0003	9.42	0.0119	
AB	0.0004	1	0.0004	12.40	0.0055	
A^2	3.567E-06	1	3.567E-06	0.0983	0.7603	
B^2	2.478E-07	1	2.478E-07	0.0068	0.9358	
A^2B	4.171E-06	1	4.171E-06	0.1150	0.7416	
AB^2	4.205E-06	1	4.205E-06	0.1159	0.7405	
A^3	0.0001	1	0.0001	3.27	0.1006	
B^3	0.0006	1	0.0006	16.13	0.0025	
Residual	0.0004	10	0.0000			
Cor Total	0.0215	19				

Table 6. Fit statistics for the cubic model

Std. Dev.	Mean	CV %	R^2	Adjusted R^2	Predicted R^2	Adeq Precision
0.0060	1.11	0.5426	0.9831	0.9679	0.9492	26.4159

A perturbation diagram compares the influence of different parameters around a specific point in the design space. The line slope is the measuring criterion. The higher the slope of a parameter is, the greater the effect of that parameter on the response variable, and the lower the slope of the parametric line, the lower the effect of that parameter on the response variable. Figure 5, representing a perturbations regarding the factors of SVF and T, illustrates that T has a smaller influence on VISR, whereas the SVF parameter had a greater effect. The outcomes mentioned align with the findings of [95].

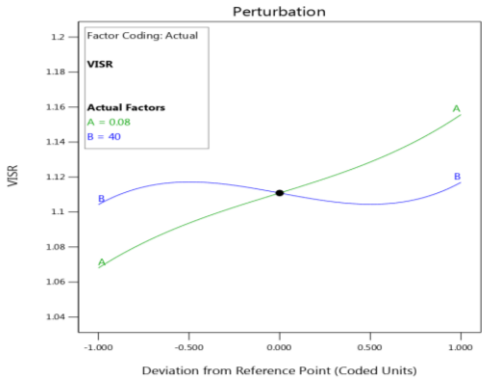

Fig. 5. Perturbation curve for effective factors

Figure 6 shows a normal probability diagram for externally studentized residuals for a cubic model. In this diagram, you can see how much the residuals deviate from the bisector line in a cubic model. The smaller the deviation of the data in a model, the higher the accuracy of that model. If the data is scattered to form an S-shaped curve, a transfer function is used to normalize the data. In other words, the closeness of data to a line can be utilized to assess the design model's appropriateness.

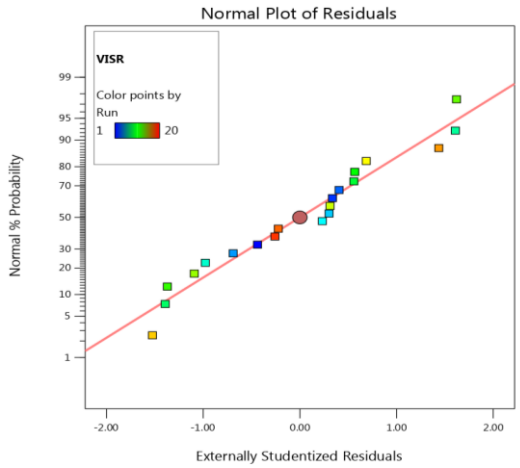

Fig. 6. Normal distribution curve versus residual values

Figure 7 illustrates the residual graph in terms of predicted values. The residual for each variable is the difference between the observed value and the predicted value for that variable. The residuals represent an error in the model and are therefore expected to have a normal distribution and be distributed in such a way that their mean value is zero. The data values conform to the criteria established by the red line. The outcomes fall within the designated range, suggesting that the developed model has functioned satisfactorily. On the other hand, residues are spread randomly along the baseline. Figure 7 shows the appropriate state for the data.

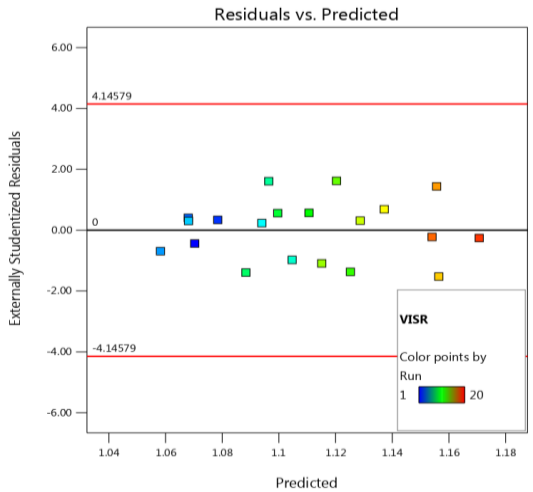

Fig. 7. Curve of predicted and remaining values

The closeness of predicted and current research result values is demonstrated in Fig. 8. Consequently, considering all three plots (Figs. 6, 7 and 8), it is justifiable to infer that the cubic equation is sufficiently reliable to form a relationship between the investigated conditions and the variables taken into account in the VISR of ZnO/EG nanofluid.

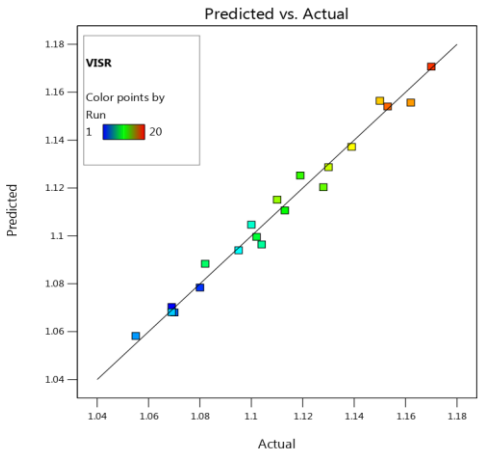

Fig. 8. Comparison of predicted and actual values for cubic model

A Box-Cox transformation is a method used to convert non-normally distributed dependent variables into a normal distribution. Box-Cox plots are used to normalize non-normal response variables. This graph is a tool to determine the most appropriate form of transfer function. In this diagram, the best lambda value, which is in the lowest part of this diagram, is determined. A lambda value of 1 in Box-Cox plot analysis signifies that the original data is a good fit. Figure 9 illustrates the Box-Cox plots associated with the cubic model. The optimal transfer function is recommended by identifying the best lambda value, which corresponds to the minimum point on the curve. If the 95% confidence interval for this lambda encompasses 1, the software will not suggest any transformation. The cubic model plot illustrated in Fig. 9 demonstrates the appropriate behavior, with the lambda line placed at the lower section of the curve.

The 2D contour and 3D surface plots in Fig. 10 (a&b) illustrates how various input parameters influence the VISR of a nanofluid. Fig. 10a displays a 2D contour demonstrating the influence of SVF and T on VISR, which aids us in comprehending the relationship between them. Fig. 10b improves deduction by presenting a three-dimensional surface plot, which facilitates a more comprehensive visualization of the intricate interactions between SVF, T, and VISR. The plot contour lines connect points with the same VISR value, allowing us to recognize areas with higher or lower VISR values and recognize any trends or patterns. The mentioned plots

show that the VISR of the nanofluid escalates rapidly as the SVF level increases. In liquids there will be molecular interactions and also additional intermolecular cohesive forces. Cohesion and molecular interchange contribute to liquid viscosity. Increasing the SVF increases the viscosity of nanofluids and it happens because of increasing friction between fluid layers [81].

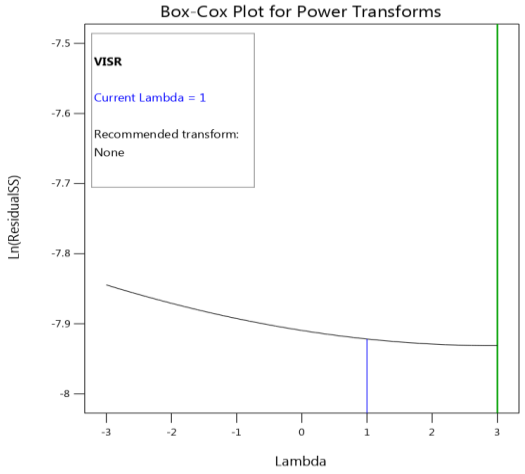

Fig. 9. Box-Cox diagrams for determining Lambda value

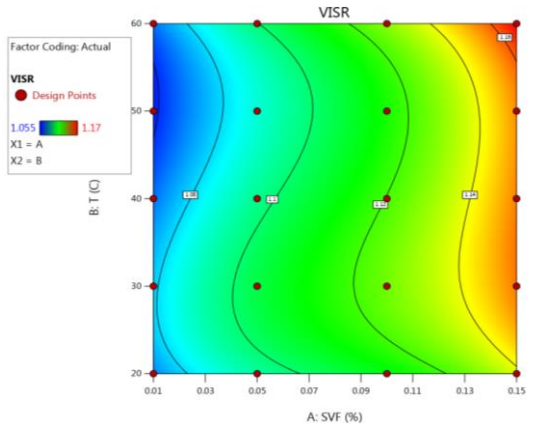

(a)

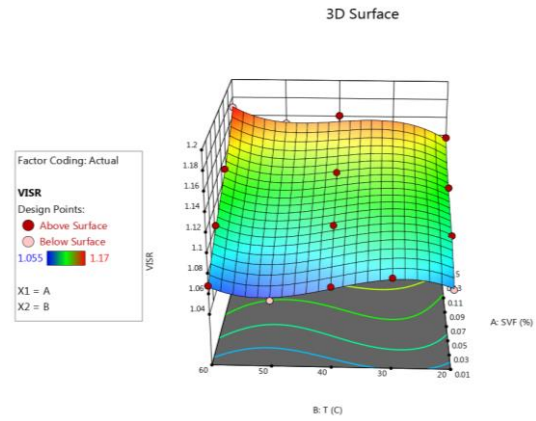

(b)

Fig. 10. Viscosity ratio of ZnO-EG nanofluid: a) 2D; b) 3D contour plotting

4.2. Optimum Response

Optimization was conducted on the VISR of the ZnO/EG nanofluid to reach its optimal value. This optimization entailed modifying the nanofluid's SVF and T. To optimize the process, the VISR of the nanofluid was minimized by employing a correlation acquired via RSM. The optimization findings showed that the nanofluid's VISR is minimized at 20 ◦C, reaching 1.070, within the investigated range of T (20 to 60 ◦C) and SVF (0.01 to 0.15% vol.). Achieving this value can only be attained when the nanofluid's SVF is set to 0. 01%. Table 7 displays various optimal solutions for nanofluids. Figure 11 (a & b) illustrates the desirable values along with the optimal VISR values at various points.

Table 7. Different optimal solutions for nanofluid

Number	SVF	T	VISR	Desirability	
1	0.010	20.000	1.070	0.954	Selected
2	0.011	20.000	1.071	0.949	
3	0.010	20.326	1.071	0.949	
4	0.010	20.788	1.072	0.942	
5	0.013	20.000	1.072	0.940	
6	0.014	20.000	1.073	0.934	
7	0.010	21.547	1.074	0.931	
8	0.016	20.000	1.075	0.925	
9	0.010	44.153	1.063	0.718	

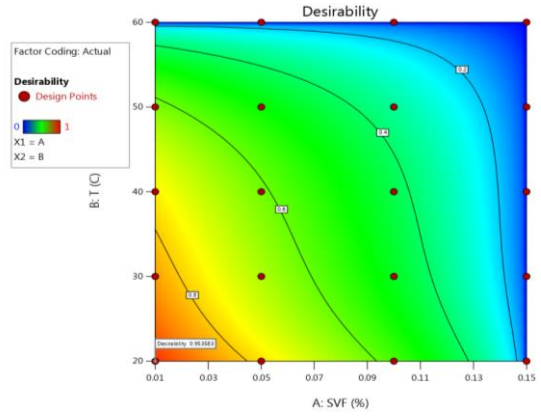

(a)

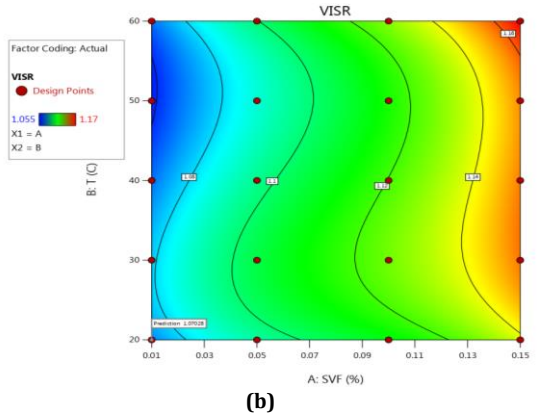

(b)

Fig. 11. Optimal values of VISR in different SVF: (a) desirability; (b) VISR

4.3. Correlations Comparison

Researchers have strongly indicated, as noted in several publications [96, 97], that new experimental-based equations are needed to establish unique models. Taking these suggestions into account, an improved correlation, Eq. (8), is formed utilizing RSM. A comparison of the calculated results with experimental data is presented in Fig. 8. The results of the current investigation, under established boundary conditions, indicate that Eq. (8) facilitates the provision of a wide range of VISR for the ZnO/EG nanofluid. This study suggests that Eq. (8) will be beneficial for researchers and help address a gap in achieving adequate results for nanofluids viscosity. Eq. (8) is derived from the utilization of ZnO nanoparticles, which possess an average particle size ranging from 10 to 30 nm, at SVF of 0.01%, 0.05%, 0.1%, and 0.15%. This study considers temperatures from 20 °C to 60 °C. The average absolute relative deviation (AARD), which pertains to the comparison of the proposed equation with other established equations, is determined in Eq (9). Table 8 shows the AARD analysis results.

$$VAARD\% = \frac{100}{N}\sum_{i=1}^{N}\frac{\left|\mu_{exp}^{i} - \mu_{eq}^{i}\right|}{\mu_{exp}^{i}} \qquad (9)$$

Table 8. Correlation comparison according to AARD

Correlation	AARD (%)
RSM (The Present Study)	2.39
Einstein [98]	9.22
Brinkman [99]	9.2
Batchelor [100]	9.21
Maiga et al. [101]	8.86
De Bruijn [102]	9.19
Hatschek [103]	9.06
Vand (a) [104]	9.07
Vand (b) [104]	9.21
Ho et al.[105]	9.01
Chen et al.[106]	8.63
Nguyen et al. (a) [107]	18.06
Nguyen et al. (b) [107]	9.37
Nguyen et al. (c) [107]	33.65
Williams et al. (a) [108]	6.1
Williams et al. (b) [108]	7.81
Godson et al.[109]	8.88
Heyhat et al.[110]	28.2
Yalcin et al. [27]	6.33
Li et al. [111]	5.15
Zyla and Fal [112]	8.3
Toghraie et al.[113]	8.46
Esfe and Saedodin [26]	9.21
Tseng and Chen[114]	59.1
Pak and Cho [115]	6.63
Abu-Nada [116]	39.44

In the existing literature, each established equation can yield acceptable outcomes within the specified constraints. Nevertheless, certain previously acquired equations cannot match the current study data. The results of the proposed procedure are compared with other equations in Fig. 12, to demonstrate the equation's applicability. Fig. 12a indicates an assessment of having AARD ≤8% equations and Fig. 12b displays a comparison of having AARD ≥ 8% equations. The figures show that some equations cannot provide accurate predictions for the current study. Li et al.'s [111] equation yields the most favorable outcome when evaluating all results. On the other hand, Abu-Nada's [116], Tseng and Chen's [114], Heyhat et al.'s [110] and Nguyen et al.'s (c) [107] equations do not exhibit any consistent alignment with the current data.

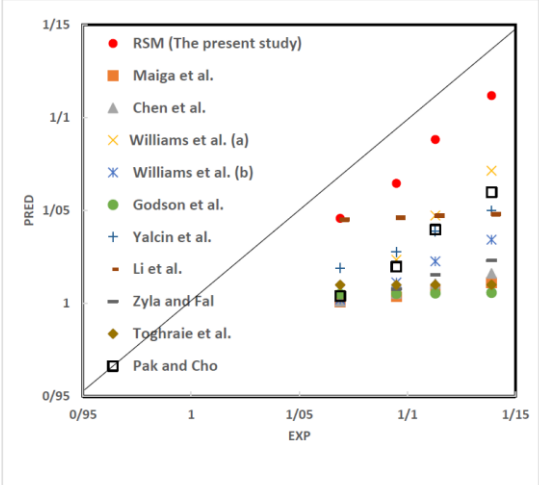

(a)

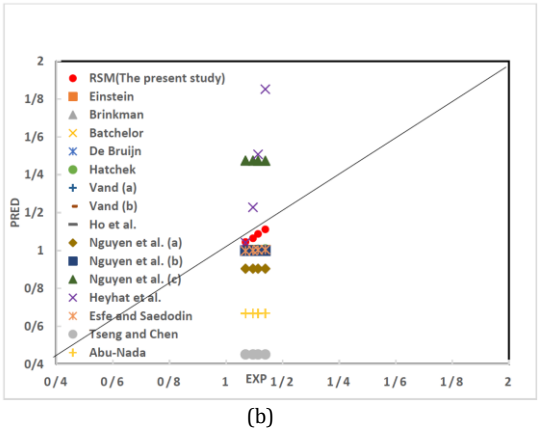

(b)

Fig. 12. Comparisons of present study equation data with other equations a) AARD ≤8% b) AARD ≥ 8%

5. Conclusions

The current research employs RSM to forecast nanofluids properties. The viscosity ratio (VISR) of ZnO/EG was examined. Various models were applied to this research, encompassing 2FI, quadratic, cubic, and quartic models. These

models were assessed according to quality indicators and plots. The cubic model has demonstrated superior performance to alternative models through the application of statistical parameters and plots. R^2, adjusted R^2, predicted R^2, std.dev and coefficient of variation parameters of the cubic model were equal to 0.9831, 0.9679, 0.9492, 0.0060 and 0.5426 respectively. This signifies the accuracy of the model. Also, the small difference of less than 0.0188 between adjusted R^2 and predicted R^2 indicates the high precision of the proposed model. The residual plot, normal probability plot, Box-Cox plot, and predicted vs. actual plot also indicated that the cubic model is highly accurate and effectively predicts the VISR of the ZnO/EG nanofluid. The RSM model findings were compared with more than 25 equations available in the literature. The outputs indicates that the RSM model had the lowest error in predicting the VISR of the nanofluid. Furthermore, the best VISR value for nanofluids was 1.070 when SVF=0.01% and T = 20 C. However, the study was not without limitations. Potential nanoparticle aggregation at higher concentrations could affect long-term stability, which was not fully explored in this work. Future research could focus on investigating these stability challenges in greater depth. It could also explore the application of this nanofluid to electronic cooling systems, internal combustion engines, and other industrial applications, building upon the results of this study.

Nomenclature

Greek symbols

λ	Lambda value

Subscripts

bf	Bbase fluid
Exp	Eexperimental
Pred	Ppredicted
2FI	Two-factor interaction
AAD	Average absolute deviation
ANOVA	Analysis of variance
ANN	Artificial neural networ
C.D	Correlation deviation
CV (%)	Coefficient of Variation
D	Dimention
DF	Degrees of Freedom
DLS	Ddynamic light scattering
EG	Ethylene glycol
GA	Genetic algorithm
GNP	Graphene nanoplatelets
GO	Graphene oxide
h	Hour
HNF	Hybrid nanofluid
ICA	Independent component analysis
KR	Thermal conductivity ration (Knf/Kbf)
MOD	Margin of deviation
MSE	Mean square error
MWCNT	Multi-walled carbon nanotubes
ND	Nanodiamond
NSGA -II	Non-dominated sorting genetic algorithm
PSO	Particle swarm optimization
R^2	Coefficient of determination [-]
RSM	Rresponse surface methodology
SR	Shear rate
Std. Dev	Standard deviation
SVF	Solid volume fraction
T	Temperature [°C]
TEM	Transmission electron microscopy
VIF	Variance Inflation Factors
U	Uncertainty
vol	Volume
W	Water

Funding Statement

This research did not receive any specific grant from funding agencies in the public, commercial, or not-for-profit sectors.

Conflicts of Interest

The author declares that there is no conflict of interest regarding the publication of this article.

Authors Contribution Statement

Behrouz Raei: Conceptualization; Formal Analysis; Numerical Implementation; Experimental Validation; Writing and Design of the Manuscript.

References

[1] Cheng, Z., et al., 2021. New insights into the effects of methane and oxygen on heat/mass transfer in reactive porous media. *International communications in heat and mass transfer*, 129, p. 105652.

[2] Zhang, X., et al., 2016. A novel aluminum–graphite dual-ion battery. *Advanced energy materials*, 6(11), p. 1502588.

[3] Zhao, T.H., Khan, M.I., Chu, Y.M., 2023. Artificial neural networking (ANN) analysis for heat and entropy generation in flow of non-Newtonian fluid between two rotating disks. *Mathematical Methods in the Applied Sciences*, 46(3), pp. 3012-3030.

[4] Chu, Y.-M., et al., 2021. Enhancement in thermal energy and solute particles using hybrid nanoparticles by engaging activation energy and chemical reaction over a parabolic surface via finite element approach. *Fractal and Fractional*, 5(3), p. 119.

[5] Hosseini Fakhrabad, A., et al., 2021. Fabrication a composite carbon paste electrodes (CPEs) modified with multi-wall carbon nano-tubes (MWCNTs/N, N-Bis (salicyliden)-1, 3-propandiamine) for

determination of lanthanum (III). *Eurasian chem. commun*, 3, pp. 627-634.

[6] Abdolvahab, R.H., Meymian, M.Z., Soudmand, N., 2020. Characterization of ZnO, Cu and Mo composite thin films in different annealing temperatures. *Chem. Methodol*., 4(3), pp. 276-284.

[7] Farhadi, B., Ebrahimi, M., Morsali, A., 2021. Microextraction and determination trace amount of propranolol in aqueous and pharmaceutical samples with oxidized multiwalled carbon nanotubes. *Chem. Methodol,* 5, pp. 227-233.

[8] Ranjbarzadeh, R., Meghdadi Isfahani, A., Hojaji, M., 2018. Experimental investigation of heat transfer and friction coefficient of the water/graphene oxide nanofluid in a pipe containing twisted tape inserts under air cross-flow. *Experimental Heat Transfer*, 31(5), pp. 373-390.

[9] Mahian, O., et al., 2021. Recent advances in using nanofluids in renewable energy systems and the environmental implications of their uptake. *Nano Energy*, 86, p. 106069.

[10] Khan, A.M., et al., 2021. Energy, environmental, economic, and technological analysis of Al-GnP nanofluid-and cryogenic LN2-assisted sustainable machining of Ti-6Al-4V alloy. *Metals*, 11(1), p. 88.

[11] Sidik, N.A.C., et al., 2016. Recent progress on hybrid nanofluids in heat transfer applications: a comprehensive review. *International communications in heat and mass Transfer*, 78, pp. 68-79.

[12] Raei, B., et al., 2017. Experimental study on the heat transfer and flow properties of γ-Al_2O_3/water nanofluid in a double-tube heat exchanger. *Journal of Thermal Analysis and Calorimetry*, 127(3), pp. 2575-2561.

[13] Raei, B., et al., 2016. Experimental investigation on the heat transfer performance and pressure drop characteristics of γ-Al_2O_3/water nanofluid in a double tube counter flow heat exchanger. *Transport Phenomena in Nano and Micro Scales*, 5(1), pp. 64-75.

[14] Mashaei, P., et al., 2016. Numerical simulation of nanofluid application in a horizontal mesh heat pipe with multiple heat sources: a smart fluid for high efficiency thermal system. *Applied Thermal Engineering,* 100, pp. 1016-1030.

[15] Raei ,B., Forced convective heat transfer of MgO/water nanofluid under constant heat flux: experimental and statistical investigation. *Challenges in Nano and Micro Scale Science and Technology*, 2021. 9(1), p. 69-80.

[16] Choi, S.U.S. 1995. Enhancing thermal conductivity of fluids with nanoparticles. In *Proceedings of the 1995 ASME International Mechanical Engineering Congress and Exposition*. New York, USA.

[17] Selimefendigil, F., Öztop, H.F., 2018. Modeling and optimization of MHD mixed convection in a lid-driven trapezoidal cavity filled with alumina–water nanofluid: Effects of electrical conductivity models. *International Journal of Mechanical Sciences,* 136, pp. 264-278.

[18] Esfe, M.H., et al., 2018. Rheological behavior characteristics of ZrO2-MWCNT/10w40 hybrid nano-lubricant affected by temperature, concentration, and shear rate: An experimental study and a neural network simulating. *Physica E: Low-dimensional systems and nanostructures.* 102, pp. 160-170.

[19] Dogonchi, A., Selimefendigil, F., Ganji, D., 2019. Magneto-hydrodynamic natural convection of CuO-water nanofluid in complex shaped enclosure considering various nanoparticle shapes. *International Journal of Numerical Methods for Heat & Fluid Flow,* 29(5), pp. 1663-1679.

[20] Selimefendigil, F., Öztop, H.F., 2022. Effects of a rotating tube bundle on the hydrothermal performance for forced convection in a vented cavity with Ag–MgO/water hybrid and CNT–water nanofluids. *Journal of Thermal Analysis and Calorimetry,* 147(1), pp. 939-956.

[21] Chamkha, A.J. ,et al., 2018. On the nanofluids applications in microchannels: a comprehensive review. *Powder technology*, 332, pp. 287-322.

[22] Pandya, N.S., et al., 2020. Heat transfer enhancement with nanofluids in plate heat exchangers: A comprehensive review. *European Journal of Mechanics-B/Fluids*. 81, pp. 173-190.

[23] Chalespari, S.K., Marzban, A., Toghraie, D., 2024. Experimental investigation of dynamic viscosity of water-based nanofluids containing tungsten oxide–multi-walled carbon nanotubes–zirconium oxide nanoparticles at mono and hybrid conditions. *Journal of Thermal Analysis and Calorimetry*.

[24] Barkhordar, A., Ghasemiasl, R., Armaghani, T., 2022. Statistical study and a complete

overview of nanofluid viscosity correlations: a new look. *Journal of Thermal Analysis and Calorimetry,* 147(13), pp. 7099-7132.

[25] Mishra, P.C., et al., 2014. A brief review on viscosity of nanofluids. *International nano letters*, 4, pp. 109-120.

[26] Esfe, M.H., Saedodin, S., 2014. An experimental investigation and new correlation of viscosity of ZnO–EG nanofluid at various temperatures and different solid volume fractions. *Experimental thermal and fluid science*, 55, pp. 1-5.

[27] Yalçın, G., et al., 2023. The influence of particle size on the viscosity of water based ZnO nanofluid. *Alexandria Engineering Journal,* 68, pp. 561-576.

[28] Li, H., et al., 2015. Experimental investigation of thermal conductivity and viscosity of ethylene glycol based ZnO nanofluids. *Applied Thermal Engineering*, 88, pp. 363-368.

[29] Pastoriza-Gallego, M., et al., 2014. Thermophysical profile of ethylene glycol-based ZnO nanofluids. *The Journal of Chemical Thermodynamics*, 73, pp. 23-30.

[30] Gamal, M., et al., 2023. Thermophysical characterization on water and ethylene glycol/water-based MgO and ZnO nanofluids at elevated temperatures: An experimental investigation. *Journal of Molecular Liquids*, 369, p. 120867.

[31] Siddiqi, H., 2022. Heat transfer and pressure drop characteristics of ZnO/DIW based nanofluids in small diameter compact channels: an experimental study, Case Stud. *Therm. Eng*. 39, p. 102441.

[32] Cabaleiro, D., et al., 2015. Transport properties and heat transfer coefficients of ZnO/(ethylene glycol+ water) nanofluids. *International Journal of Heat and Mass Transfer,* 89, pp. 433-443.

[33] Sharma, R., et al., 2022. Characterization of ZnO/nanofluid for improving heat transfer in thermal systems. *Materials Today: Proceedings,* 62, pp. 1904-1908.

[34] Jeong, J., et al., 2013. Particle shape effect on the viscosity and thermal conductivity of ZnO nanofluids. *International journal of refrigeration*, 36(8), pp. 2233-2241.

[35] Rostamian, H., Lotfollahi, M.N., 2015. A new simple equation of state for calculating solubility of solids in supercritical carbon dioxide. *Periodica Polytechnica Chemical Engineering*, 59(3), pp. 174-185.

[36] Esfe, M.H., et al., 2015. Applicability of artificial neural network and nonlinear regression to predict thermal conductivity modeling of Al_2O_3–water nanofluids using experimental data. *International Communications in Heat and Mass Transfer,* 66, pp. 246-249.

[37] Dalkilic, A., et al., 2016. Prediction of graphite nanofluids' dynamic viscosity by means of artificial neural networks. *International Communications in Heat and Mass Transfer*, 73, pp. 33-42.

[38] Esfe, M.H., et al., 2015. Designing an artificial neural network to predict thermal conductivity and dynamic viscosity of ferromagnetic nanofluid. *International Communications in Heat and Mass Transfer*, 68, pp. 50-57.

[39] Esfe, M.H., et al., 2022. The effect of different parameters on ability of the proposed correlations for the rheological behavior of SiO2-MWCNT (90: 10)/SAE40 oil-based hybrid nano-lubricant and presenting five new correlations. *ISA transactions*, 128, pp. 488-497.

[40] Hemmat Esfe, M., Saedodin, S., 2022. Investigating the Behavior of SiO2 (90%)-MWCNT (10%)/SAE50 Hybrid Nanofluid and Modeling its Viscosity. *Arabian Journal for Science and Engineering,* pp. 1-12.

[41] Esfe, M.H., et al., 2023. Using the RSM to evaluate the rheological behavior of SiO2 (6-(٪ٔMWCNT (40%)/SAE40 oil hybrid nanofluid and investigating the effect of different parameters on the viscosity. *Tribology International*, 184, p. 108479.

[42] Baghoolizadeh, M., et al., 2023. Using different machine learning algorithms to predict the rheological behavior of oil SAE40-based nano-lubricant in the presence of MWCNT and MgO nanoparticles. *Tribology International*, 187, p. 108759.

[43] Demirpolat, A.B., Baykara, M., 2021. Investigation and prediction of ethylene Glycol based ZnO nanofluidic heat transfer versus magnetic effect by deep learning. *Thermal Science and Engineering Progress,* 25, p. 101034.

[44] Baghoolizadeh, M., et al., 2024. Prediction and extensive analysis of MWCNT-MgO/oil SAE 50 hybrid nano-lubricant rheology utilizing machine learning and genetic algorithms to find ideal attributes. *Tribology International*, 195, p. 109582.

[45] Song, X., et al., 2024. Utilizing machine learning algorithms for prediction of the

rheological behavior of ZnO (50%)-MWCNTs (50%)/Ethylene glycol (20%)-water (80%) nano-refrigerant. *International Communications in Heat and Mass Transfer*, 156, p. 107634.

[46] Hussein, S.A., et al., 2024. Applying different machine learning algorithms to predict the viscosity behavior of MWCNT–alumina/water–ethylene glycol (20: 80) hybrid antifreeze. *International Journal of Thermofluids,* 24, p. 100966.

[47] Graish, M.S., et al., 2025. Prediction of the viscosity of iron-CuO/water-ethylene glycol non-Newtonian hybrid nanofluids using different machine learning algorithms. *Case Studies in Chemical and Environmental Engineering*, 11, p. 101180.

[48] Shekhar, et al., 2025. Predicting nanofluid density in ethylene glycol-based oxide nanoparticles using machine learning approach: GBR–GSO models. *Journal of Thermal Analysis and Calorimetry*.

[49] Demirpolat, A.B., Uyar, M.M., Arslanoğlu, H., 2025, Heat transfer with MgO nanofluid in laminar flow: experimental study and ANSYS modeling. *Journal of Thermal Analysis and Calorimetry*, 150(1), pp. 813-820.

[50] Mahanta, C., Sharma, R.P., 2025. Contrasting analysis of tetra and ternary nanofluid dynamics over linear/exponential stretching sheets with variable thermal conductivity: an RSM approach. *Journal of Thermal Analysis and Calorimetry*, 150(1), pp. 649-671.

[51] Mahanta, C., Sharma, R.P., 2025. Enhanced heat transfer rate analysis with Ohmic heating, and multiple slips over exponentially stretching/shrinking plate on MHD hybrid nanofluid: Response surface methodology. *ZAMM-Journal of Applied Mathematics and Mechanics/Zeitschrift für Angewandte Mathematik und Mechanik*, p. e202400479.

[52] Kumar, V.V., Sharma, R.P., 2025. Entropy generation minimization in nuclear reactor cooling via rough rotating disk: a statistical approach. *Multiscale and Multidisciplinary Modeling, Experiments and Design,* 8(5), p. 245.

[53] Sharma, A., Sharma, R.P., 2025. Statistical and numerical analysis of MHD nanofluid (TiO2/EG) flow on a nonlinear curved stretching surface with heat source: A RSM approach. *ZAMM-Journal of Applied Mathematics and Mechanics/Zeitschrift für Angewandte Mathematik und Mechanik,* 105(1), p. e202400513.

[54] Shamshuddin, M.D., Prakash Sharma, R., 2023. Thermal elaboration of ethylene glycol-based magnetized nanostructures via a convective permeable heated vertical surface employing modified Buongiorno model. *Journal of Magnetism and Magnetic Materials*, 571, p. 170588.

[55] Mondal, S., Ghosh, R., Sharma, R.P., 2023. Entropy Generation Effects on Hydromagnetic Williamson Nanofluid Flow through a Porous Media. *Nanoscience & Nanotechnology-Asia*, 13(1).

[56] Prakash, O., et al., 2023. Hybrid nanofluid MHD motion towards an exponentially stretching/shrinking sheet with the effect of thermal radiation, heat source and viscous dissipation. *Pramana*, 97(2), p. 64.

[57] Swain, L., Sharma, R.P., Mishra, S., 2025. Analysis of bio-convection-driven conducting flow of Williamson nanofluid through an expanding surface with activation energy. *Journal of Thermal Analysis and Calorimetry*.

[58] Sharma, R.P., et al., 2024. Significance of homogeneous–heterogeneous reaction on MHD nanofluid flow over a curvilinear stretching surface. *Pramana*, 98(4), pp. 1-11.

[59] Sharma, R.P., et al., 2024. Impact of radiation, melting, and chemical reaction on magnetohydrodynamics nanoparticle aggregation flow across parallel plates. *Journal of Central South University*, 31(10), pp. 3715-3729.

[60] Sharma, R.P., et al., 2024. Influence of heat source/sink on a rotating cone in a rotating nanofluid with magnetic field impact: Application of Hosoya polynomial-based collocation method. *ZAMM-Journal of Applied Mathematics and Mechanics/Zeitschrift für Angewandte Mathematik und Mechanik*, 104(9), p. e202400294.

[61] Mishra, S.R., Sharma, R.P., Swain, L., 2024. Illustration of Joule dissipation on the time-dependent stagnation point flow of nanofluid through a porous surface. *International Journal of Modern Physics B*, 38(05), p. 2450077.

[62] Shamshuddin, M.D., et al., 2024. Induced magnetic transportation of Soret and dissipative effects on Casson fluid flow towards a vertical plate with thermal and species flux conditions. *International Journal of Modern Physics B*, 38(11), p. 2450157.

[63] Sharma, R.P., et al., 2024. Illustration of thermal radiation on the mixed convection of Williamson nanofluid over an inclined cylindrical surface. *Modern Physics Letters B,* 38(25), p. 2450141.

[64] Sharma, R.P., Gorai, D., 2024. Unveiling the dynamic symphony of melting heat transfer in the flow between a stretching Riga plate and a squeezing plate. *International Communications in Heat and Mass Transfer*, 156, p. 107565.

[65] Shukla, S., et al., 2024. Investigation of thermodynamics characteristics of ternary hybrid nanofluid flow over a stretching sheet. *Modern Physics Letters B*, 38(12), p. 2450079.

[66] Chu, Y.-M., et al., 2021. Examining rheological behavior of MWCNT-TiO2/5W40 hybrid nanofluid based on experiments and RSM/ANN modeling. *Journal of Molecular Liquids*, 333, p. 115969.

[67] Demirpolat, A.B., Das, M., 2019. Prediction of viscosity values of nanofluids at different pH values by alternating decision tree and multilayer perceptron methods. *Applied Sciences*, 9(7), p. 1288.

[68] Esfe, M.H., Arani, A.A.A., 2018. An experimental determination and accurate prediction of dynamic viscosity of MWCNT (% 40)-SiO2 (% 60)/5W50 nano-lubricant. *Journal of Molecular Liquids,* 259, pp. 227-237.

[69] Demirpolat, A.B., Das, M., 2020. Cuo ve Zno İçeren Nanoakışkanların Termofiziksel Özelliklerinin Belirlenmesi ve Yapay Sinir Ağı İle Modellenmesi. *Dicle Üniversitesi Mühendislik Fakültesi Mühendislik Dergisi,* 11(1), pp. 225-238.

[70] Demirpolat, A.B., Daş, M., 2018. (Cuo) copper oxide nanoparticle production and determination of heat transfer coefficient. *American Journal of Engineering Research (AJER)*, 7(11), pp. 74-80.

[71] Baghoolizadeh, M., et al., 2024. Using of artificial neural networks and different evolutionary algorithms to predict the viscosity and thermal conductivity of silica-alumina-MWCN/water nanofluid. *Heliyon*, 10(4).

[72] Rostamzadeh-Renani, R., et al., 2023. Prediction of the thermal behavior of multi-walled carbon nanotubes-CuO-CeO2 (20-40-40)/water hybrid nanofluid using different types of regressors and evolutionary algorithms for designing the best artificial neural network modeling. *Alexandria Engineering Journal*, 84, p. 184-203.

[73] Jin, W., et al., 2024. Regression modeling and multi-objective optimization of rheological behavior of non-Newtonian hybrid antifreeze: Using different neural networks and evolutionary algorithms. *International Communications in Heat and Mass Transfer*, 155, p. 107578.

[74] Zhou, H., et al., 2024. Combination of group method of data handling neural network with multi-objective gray wolf optimizer to predict the viscosity of MWCNT-TiO2-oil SAE50 nanofluid. Case Studies in Thermal Engineering, 64, p. 105541.

[75] Refaish, A.H., et al., 2025. Using Different Evolutionary Algorithms and Artificial Neural Networks to Predict the Rheological Behavior of a New Nano-lubricant Containing Multi-walled carbon nanotube and zinc oxide Nano-powders in Oil 10W40 Base Fluid. *International Journal of Thermofluids,* p. 101092.

[76] Rostamzadeh-Renani, R., et al., 2024. Multi-objective optimization of rheological behavior of nanofluids containing CuO nanoparticles by NSGA II, MOPSO, and MOGWO evolutionary algorithms and Group Method of Data Handling Artificial neural networks. *Materials Today Communications,* 38, p. 107709.

[77] Hemmat Esfe, M., et al., 2024. Investigating the viscosity of hybrid nano-lubricant containing MWCNTs with ANN modeling to introduce the best and most optimal lubricant. *Journal of Thermal Analysis and Calorimetry,* 149(10), p. 4561-4573.

[78] Gao, J., et al., 2024. An RBF-based artificial neural network for prediction of dynamic viscosity of MgO/SAE 5W30 oil hybrid nano-lubricant to obtain the best performance of energy systems. *Materials Today Communications,* 38, p. 107836.

[79] Arjmandi, H., Amiri, P., Pour, M.S., 2020. Geometric optimization of a double pipe heat exchanger with combined vortex generator and twisted tape: A CFD and response surface methodology (RSM) study. *Thermal Science and Engineering Progress*, 18, p. 100514.

[80] Ma, M., et al., 2020. Statistical image analysis of uniformity of hybrid nanofluids and prediction models of thermophysical parameters based on artificial neural network (ANN). *Powder Technology*, 362, pp. 257-266.

[81] Esfe, M.H., et al., 2018. Prediction and optimization of thermophysical properties of stabilized Al_2O_3/antifreeze nanofluids using response surface methodology. *Journal of Molecular Liquids*, 261, pp. 14-20.

[82] Esfe, M.H., Motallebi, S.M., Toghraie, D., 2022. Optimal viscosity modelling of 10W40 oil-based MWCNT (40%)-TiO2 (60%) nanofluid using Response Surface Methodology (RSM). *Heliyon*, 8(12).

[83] Esfe, M.H., Motallebi, S.M., Toghraie, D., 2022. Modeling and optimization of dynamic viscosity of oil-based nanofluids containing alumina particles and carbon nanotubes by response surface methodology (RSM). *Korean Journal of Chemical Engineering*, 39(10), p. 2800-2809.

[84] Khetib, Y., et al., 2023. Competition of ANN and RSM techniques in predicting the behavior of the CuO-liquid paraffin. *Chemical Engineering Communications*, 210(6), pp. 880-892.

[85] Esfe, M.H., et al., 2024. Applying knowledge management in optimal modeling of viscosity of nanofluids by response surface methodology for use in automobiles engine. *Materials Today Communications*, 39, p. 108897.

[86] Hemmat Esfe, M., et al., 2025. Experimental study of thermal conductivity of SWCNT–TiO2–CuO (10: 70: 20)/water ternary hybrid nanofluid (THNF) and providing a new equation using response surface methodology. *Journal of Thermal Analysis and Calorimetry*, p. 1-13.

[87] Li, J., et al., 2024. Multi-objective optimization of a laterally perforated-finned heat sink with computational fluid dynamics method and statistical modeling using response surface methodology. *Engineering Applications of Artificial Intelligence*, 130, p. 107674.

[88] Qamar, A., et al., 2020. Preparation and dispersion stability of aqueous metal oxide nanofluids for potential heat transfer applications: a review of experimental studies. *Journal of Thermal Analysis and Calorimetry,* 2020, pp. 1-24.

[89] Li, X., Zhu, D., Wang, X., 2007. Evaluation on dispersion behavior of the aqueous copper nano-suspensions. *Journal of colloid and interface science*, 310(2), pp. 456-463.

[90] Raei, B., Peyghambarzadeh, S.M., 2019. Measurement of Local Convective Heat Transfer Coefficient of Alumina-Water Nanofluids in a Double Tube Heat Exchanger. *Journal of Chemical and Petroleum engineerin*g, 53(1), pp. 25-36.

[91] Wei, X., Wang, L., 2010. Synthesis and thermal conductivity of microfluidic copper nanofluids. *Particuology*, 8(3), pp. 262-271.

[92] Teng, T.-P., et al., 2010. The effect of alumina/water nanofluid particle size on thermal conductivity. *Applied Thermal Engineering*, 30(14-15), p. 2213-2218.

[93] Saeedi, A.H., Akbari, M., Toghraie, D., 2018. An experimental study on rheological behavior of a nanofluid containing oxide nanoparticle and proposing a new correlation. *Physica E: Low-dimensional Systems and Nanostructure*s, 99, p. 285-293.

[94] Lau, H.-L., et al., 2023. Optimization of fermentation medium components by response surface methodology (RSM) and artificial neural network hybrid with genetic algorithm (ANN-GA) for lipase production by Burkholderia cenocepacia ST8 using used automotive engine oil as substrate. *Biocatalysis and Agricultural Biotechnology*, 50, p. 102696.

[95] Elcioglu, E.B., et al., 2018. Experimental study and Taguchi Analysis on alumina-water nanofluid viscosity. *Applied Thermal Engineering*, 128, pp. 973-981.

[96] Aybar, H.Ş., et al., 2015. A review of thermal conductivity models for nanofluids. *Heat Transfer Engineering,* 36(13), pp. 1085-1110.

[97] Yıldız, Ç., Arıcı, M., Karabay, M., 2019. Comparison of a theoretical and experimental thermal conductivity model on the heat transfer performance of Al_2O_3-SiO2/water hybrid-nanofluid. *International Journal of Heat and Mass Transfer,* 140, pp. 598-605.

[98] Einstein, A., 1906. A new determination of the molecular dimensions. *Ann.physics*, 19, pp. 289-306.

[99] Brinkman, H.C., 1952. The viscosity of concentrated suspensions and solutions. *The Journal of chemical physics*, 20(4), p. 571.

[100] Batchelor, G., 1977. The effect of Brownian motion on the bulk stress in a suspension of spherical particles. *Journal of fluid mechanics,* 83(1), pp. 97-117.

[101] Maïga, S.E.B., et al., 2004. Heat transfer behaviours of nanofluids in a uniformly heated tube. *Superlattices and Microstructures*, 35(3-6), p. 543-557.

[102] De Bruijn, H., 1942. The viscosity of suspensions of spherical particles (The fundamental η-c and φ relations). *Recueil des Travaux Chimiques des Pays-Bas*, 61(12), pp. 863-874.

[103] Hatschek, E., 1913. The general theory of viscosity of two-phase systems. *Transactions of the Faraday Society*, 9, p. 80-92.

[104] Vand, V., 1945. Theory of viscosity of concentrated suspensions. *Nature*, 155(3934), pp. 364-365.

[105] Ho, C., et al., 2010. Natural convection heat transfer of alumina-water nanofluid in vertical square enclosures: an experimental study. *International Journal of Thermal Sciences*, 49(8), pp. 1345-1353.

[106] Chen, H., et al., 2007. Rheological behaviour of ethylene glycol based titania nanofluids. *Chemical physics letters*, 444(4-6), pp. 333-337.

[107] Nguyen, C., et al., 2007. Temperature and particle-size dependent viscosity data for water-based nanofluids–hysteresis phenomenon. *International journal of heat and fluid flow*, 28(6), pp. 1492-1506.

[108] Williams, W., Buongiorno, J., Hu, L.W., 2008. Experimental investigation of turbulent convective heat transfer and pressure loss of alumina/water and zirconia/water nanoparticle colloids (nanofluids) in horizontal tubes. *Journal of Heat Transfer*, 130(4), p. 042412.

[109] Godson, L., et al., 2010. Experimental investigation on the thermal conductivity and viscosity of silver-deionized water nanofluid. *Experimental Heat Transfer,* 23(4), pp. 317-332.

[110] Heyhat, M., et al., Experimental investigation of turbulent flow and convective heat transfer characteristics of alumina water nanofluids in fully developed flow regime. *International Communications in Heat and Mass Transfer,* 2012. 39(8), p. 1272-1278.

[111] Li, F., et al., 2019. Effects of ultrasonic time, size of aggregates and temperature on the stability and viscosity of Cu-ethylene glycol (EG) nanofluids. *International Journal of Heat and Mass Transfer*, 129, pp. 278-286.

[112] Żyła, G., Fal, J., 2017. Viscosity, thermal and electrical conductivity of silicon dioxide–ethylene glycol transparent nanofluids: An experimental studies. *Thermochimica acta,* 650, pp. 106-113.

[113] Toghraie, D., Alempour, S.M., Afrand, M., 2016. Experimental determination of viscosity of water based magnetite nanofluid for application in heating and cooling systems. *Journal of Magnetism and Magnetic Materials*, 417, pp. 243-248.

[114] Tseng, W.J., Chen, C.-N., 2003. Effect of polymeric dispersant on rheological behavior of nickel–terpineol suspensions. *Materials Science and Engineering: A*, 347(1-2), pp. 145-153.

[115] Pak, B.C., Cho, Y.I., 1998. Hydrodynamic and heat transfer study of dispersed fluids with submicron metallic oxide particles. *Experimental Heat Transfer an International Journal*, 11(2), pp. 151-170.

[116] Abu-Nada, E., 2009. Effects of variable viscosity and thermal conductivity of Al_2O_3–water nanofluid on heat transfer enhancement in natural convection. *International Journal of Heat and Fluid Flow*, 30(4), pp. 679-690.